Title	Effects of corrugated aerofoil surface features on flow separation control.
Author(s)	New, T. H.; Chan, Y. X.; Koh, G. C.; Hoang, M. C.; Shi, Shengxian.
Citation	New, T. H., Chan, Y. X., Koh, G. C., Hoang, M. C., & Shi, S. (2013). Effects of Corrugated Aerofoil Surface Features on Flow-Separation Control. AIAA Journal, 52(1), 206-211.
Date	2013
URL	http://hdl.handle.net/10220/18779
Rights	© 2013 American Institute of Aeronautics and Astronautics, Inc. This is the author created version of a work that has been peer reviewed and accepted for publication by AIAA Journal, American Institute of Aeronautics and Astronautics, Inc. It incorporates referee's comments but changes resulting from the publishing process, such as copyediting, structural formatting, may not be reflected in this document. The published version is available at DOI: [http://dx.doi.org/10.2514/1.J052398].

Effects of corrugated aerofoil surface features on flow separation control

T. H. New[1], Y. X. Chan[1], G. C. Koh[1], M. C. Hoang[2] and Shengxian Shi[3]

[1]*Nanyang Technological University, 50 Nanyang Avenue, 639798, Singapore*

[2]*NUS High School of Maths and Science, 20 Clementi Avenue 1, 129957, Singapore*

[3]*Key Laboratory for Power Machinery and Engineering of Ministry of Education, School of Mechanical Engineering, Shanghai Jiao Tong University, 200240, Shanghai, China*

1. Introduction

With increased awareness of the potential engineering benefits in emulating certain aspects of insect-wings or insect flight mechanics, it is not surprising that there is recent surge of interest in their investigations for lift generation or stall mitigation. Other than exploring how the exact flapping/heaving mechanisms employed by insects contribute towards their agility during flight [1-8], understanding how unique surface geometries and features of insect wings enable these insects to maneuver the way they do is also one of the major research motivations for some recent studies. Of interest to the present study are investigations conducted by Hu and Tamai [9], Murphy and Hu [10] and Levy and Seifert [11] recently, where they looked at the flow dynamics of aerofoils based on dragonfly wing cross-sections. References [9] and [10] studied corrugated aerofoils with cross-sections resembling typical dragonfly wing cross-sections and observed favourable aerodynamic behaviour. They noted that flow separation vortices trapped within the corrugation valleys draw fluid towards the aerofoil wall region and reduce the overall extent of the flow separation region. These unique flow features mean that flow separations can be delayed till a higher angle-of-attack with accompanying increases in lift-to-drag ratios for these corrugated aerofoils up to a chord Reynolds numbers of Re=125,000.

On the other hand, the corrugated aerofoil studied by Ref. [11] had far fewer corrugations. Instead, their aerofoil has only two corrugations close to the leading-edge, followed by a “saddle” and convex trailing-edge “hump”. Due to this geometric difference, the mechanisms with which this aerofoil is able to delay flow separation are different. In this case, flow separations arising from the upstream corrugations reattach back to trailing-edge hump regularly, which translates into fewer flow separation

events propagating beyond the trailing-edge. In particular, a recirculating vortex is observed to form at the saddle, which is believed to play an important role in controlling flow separation. It should be mentioned that Ref. [9] performed their experiments at Re=34,000, Ref. [10] conducted theirs at Re=58,000 to 125,000, while Ref. [11] performed their investigations at Re<8000. In addition, the ranges of angle-of-attack investigated between these studies were also different.

It is clear from the earlier studies that the vortex formation and behaviour along the upper surfaces of corrugated aerofoils drive the favourable flow effects seen so far. While some insights into their behaviour have been provided by the earlier studies, direct comparisons between them were difficult due to the different test conditions used. To do that, they have to be studied under similar flow conditions and this provided the primary motivation for the present study. To accomplish that, an experimental flow visualization and particle-image velocimetry (PIV) investigation was performed in this study to compare the differences in the near-field vortical behaviour and the extent to which flow separation is mitigated between these two corrugated aerofoils at a fixed chord Reynolds number of Re=14,000. The use of a relatively low Reynolds number here will not only provide additional insights into the basic aerodynamic characteristics of dragonfly wings, but also shed light on the use of different corrugated aerofoils in micro-aerial vehicles (i.e. MAVs) as well.

2. Experimental setup

The experiments were conducted in a low-speed recirculating water tunnel with a test-section measuring 450mm (W) x 600mm (H) x 1500mm (L). The test-section was constructed from glass which allowed good optical access from the sides and bottom. Water was recirculated throughout the water tunnel by an axial pump and it was conditioned using honeycombs, fine screens and a contraction section before entering the test-section. The experimental setup used here is shown in Fig. 1, where two flat end-plates were located at both ends of the 300mm long, 75mm chord test aerofoils. A stepper motor was used to vary the aerofoil angle-of-attack and attached to the aerofoils via a coupling at their quarter-chord locations. The Reynolds number used during the experiments was approximately $Re=Uc/\nu=14,000$, where U is the mean free stream velocity, c is the aerofoil chord length and ν is water kinematic viscosity at working conditions. Free-stream turbulence intensity was estimated to be 1.1% at the working free-stream velocity of U=0.19m/s, as determined from time-

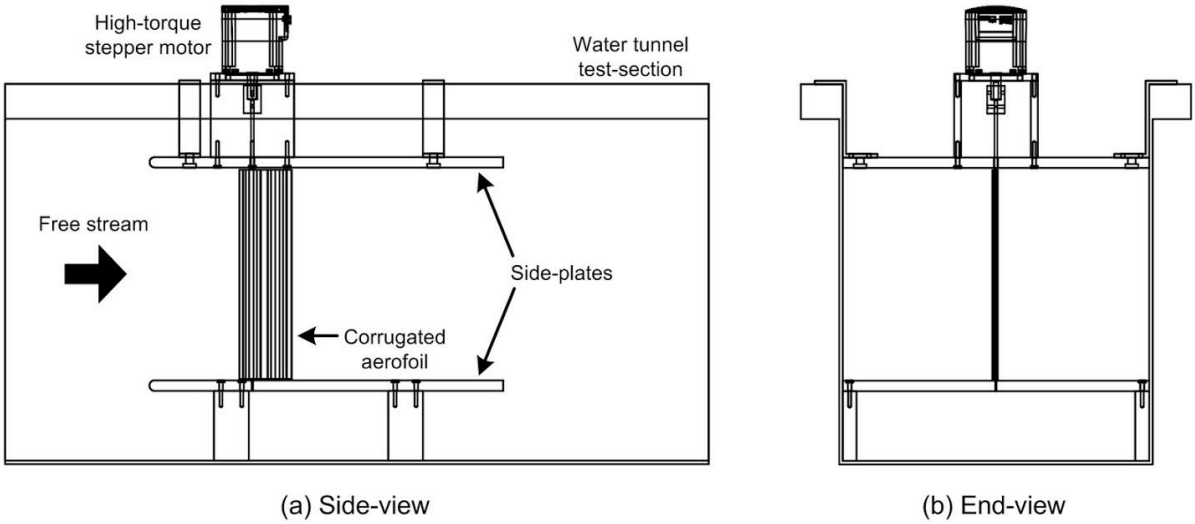

Fig. 1 Experimental apparatus and setup used in the present study

averaged PIV measurements taken at the region where the aerofoils were to be mounted. Lastly, uncertainty in the free stream Reynolds number has also been ascertained to be approximately ±1.2%.

Two different corrugated aerofoils were studied: the first one was based on a typical dragonfly wing cross-section investigated by Refs. [9] and [10], while the second one was based on a simplified dragonfly wing cross-section studied by Ref. [11]. To ease identification of the aerofoils here, they will be known as Corrugated A and B respectively. As indicated in Fig. 2, the design of Corrugated A aerofoil consisted of a series of non-uniform sharp peaks and valleys. On the other hand, Corrugated B aerofoil had two identical sharp peaks with a valley in-between, followed by a rather significant but smooth hump. Geometries of the present corrugated aerofoils were designed according to the design rules provided in the above studies and therefore, their detailed design rules will not be elaborated. The leading-edge and trailing-edge thicknesses of Corrugated A aerofoil were 3mm, while those of Corrugated B were 2mm. For the sake of comparison, a symmetrical NACA0010 aerofoil was tested alongside with the corrugated aerofoils. It was selected as the maximum thickness-to-chord ratios for both corrugated aerofoils were approximately 10%, comparable to that of the NACA0010 aerofoil. All aerofoil test models had spans and chords of b=300mm and c=75mm respectively, which yielded a consistent aspect-ratio of b/c=4 throughout the study. This aspect-ratio is higher than that in Hu and Tamai (2008) and Murphy and Hu (2010), where aspect-ratio of $b/c \approx 3$ aerofoils were investigated, as well as Levy and Seifert (2009) where a relatively low aspect-ratio of $b/c \approx 2$ aerofoil was studied.

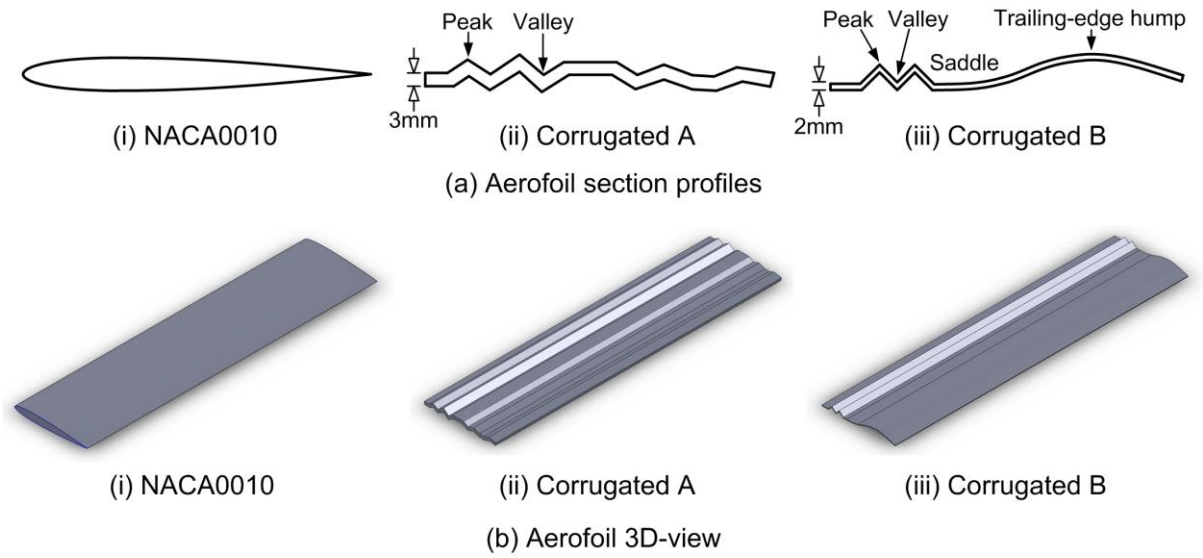

Fig. 2 Cross-section profiles and 3D-views of the reference NACA0010 and two corrugated aerofoils

Since higher aspect-ratio aerofoils are much less likely to result in three-dimensional effects arising from the end-walls and mounting mechanisms (i.e. at one of the end walls, in this case) than lower aspect-ratio aerofoils, the flow behaviour observed along the mid-span of the test aerofoils here will be representative.

Note that unlike the NACA0010 aerofoil, both Corrugated A and B aerofoils had different non-zero cambers. However, it is worthwhile to point out that the overall cambers of the two corrugated aerofoils were dissimilar to begin with, thus posing significant technical challenges and complexities when attempting to compare based on the notion of equivalent camber. On the other hand, making use of a similar maximum thickness-to-chord ratio was found to be more appropriate instead, since it is still one of the most important geometrical characteristics of an aerofoil that affects flow separation behaviour. Lastly, all test aerofoils were fabricated from stainless steel blocks using wire-cutting technique, with their surfaces smoothed down using sandpaper and spray-painted matt black for the experiments.

Particle-streak visualizations were used to give a first-hand appreciation of the flow fields produced by the three aerofoils. In this case, 20micron polyamide seeding particles were uniformly distributed within the water-tunnel and a digital DSLR camera with an f1.8, 50mm manual lens located beneath the transparent water tunnel floor was used to capture the flow fields. To provide illumination, a 1W

LaVision 532nm continuous-wave laser was used in conjunction with beam-steering and sheet-forming optics, such that the laser sheet was aligned along the mid-span of the test aerofoils. The laser sheet was approximately 1.5mm thick. Global velocity measurements of the flow fields were conducted using a 2D PIV system. It comprised of a 200mJ double-pulse Nd:YAG laser with sheet-forming optics, a 1600px by 1200px double-frame CCD camera with a f2.8, 28mm lens attached, with synchronizing and image-grabbing cards housed in a workstation. The measurement plane was similar to the flow visualization plane used earlier. 20micron polyamid seeding particles were premixed into the water-tunnel and double-frame, single exposure images of scattered light from the particles were captured by the system at 15Hz. A total of one thousand image-pairs (i.e. instantaneous velocity fields) were captured for each aerofoil at every angle-of-attack used to ensure satisfactory convergence in the mean flow field characteristics.

The physical PIV measurement window was approximately 126.9mm x 95.3mm and maintained throughout the study. All double-frame images were processed using multi-grid cross-correlation with initial and final interrogation window sizes of $128px^2$ and $32px^2$ (i.e. approximately $10.2mm^2$ and $2.5mm^2$ respectively) and 50% window-overlapping in both directions. Based on the PIV measurement procedures, velocity vector map resolution was approximately 1.25mm/vector. As the PIV experiments were performed according to the procedures recommended by Keane and Adrian [12], uncertainty levels of the measured velocity components were limited to within ±1%. Lastly, Proper Orthogonal Decomposition (POD) analysis was performed on the PIV velocity fields to reconstruct the vorticity fields based on the first 50 modes, which took into account 86% of the flow energy. This was performed to better differentiate the dominant flow structures from the incoherent turbulent flow structures, such that effects of the aerofoil surface geometries on the overall flow separation behaviour can be properly isolated. The methodology used in the POD analysis here followed those described by Sirovich (1987), Berkooz et al. (1993) and Chatterjee (2000), where sequential vorticity fields were decomposed into corresponding sets of POD coefficients and eigenfunctions or modes. Since these POD coefficients and modes correspond to different flow structures with dissimilar length-scales, this technique is particularly useful in isolating the behaviour of coherent and incoherent flow structures associated with complex flow fields. For the sake of brevity, readers are advised to refer to Lumley (1967), Aubry et al. (1988), Arndt et al. (1997), Kim

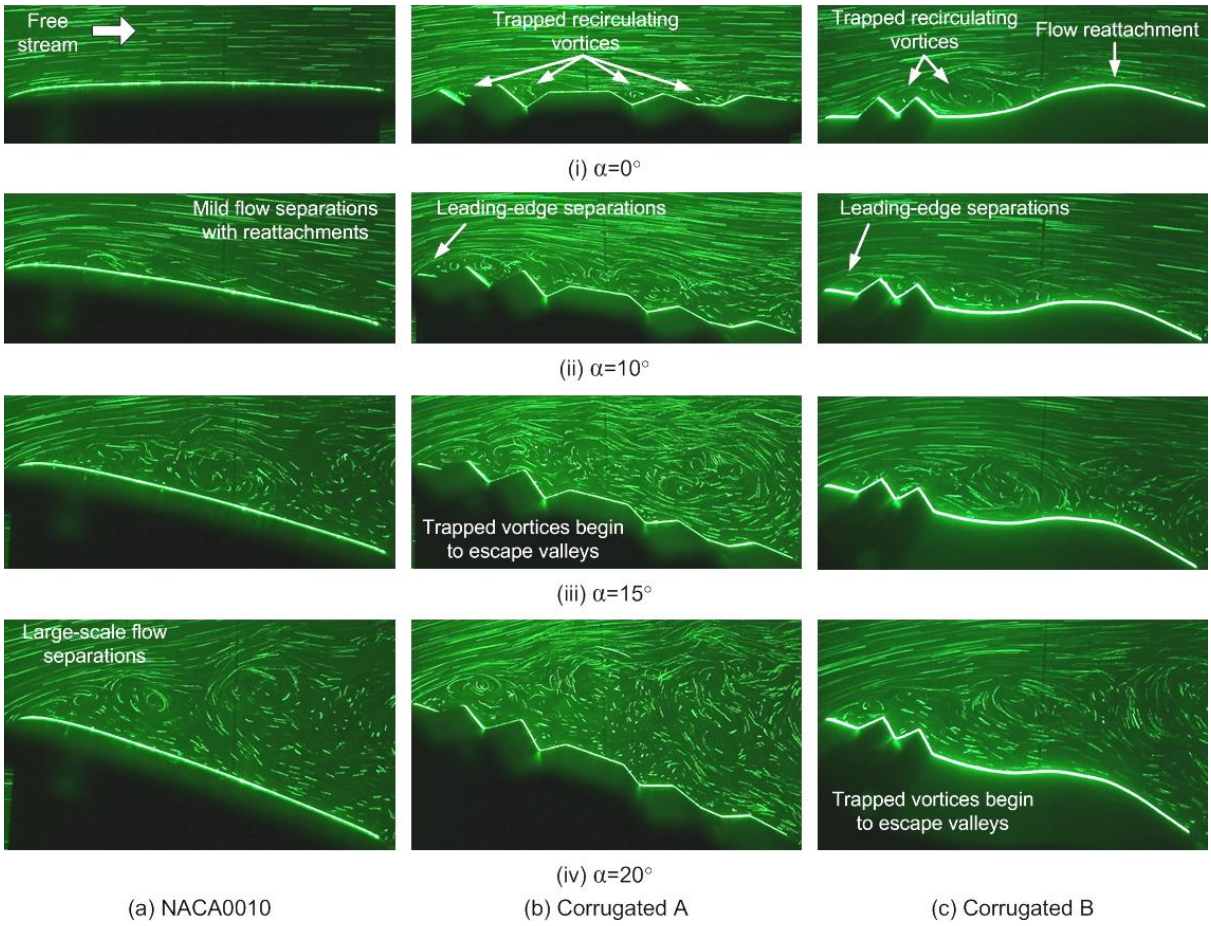

Fig. 3 Visualized instantaneous flow fields along the upper surface of (a) NACA0010, (b) Corrugated A and (c) Corrugated B aerofoils at α=0°, 10°, 15° and 20°.

and Rockwell (2005) and Shi et al. (2013) for more details on the POD technique.

3. Results and Discussions

(i) Near-field vortex structures and behaviour

To shed light upon the near-field vortex structures and their behaviour along the upper surfaces of the corrugated aerofoils, particle-streak visualizations and reconstructed vorticity fields taken at α=0°, 10°, 15° and 20° are presented in Figs. 3 and 4. To begin with, for the reference NACA0010 aerofoil presented in Figs. 3(a) and 4(a), no discernible flow separations can be detected along the aerofoil surface at α=0°, though mild flow separations that reattach back to the aerofoil surface can be seen to occur at α=10°. As the angle-of-attack increases further to α=15° and 20°, flow separation regions become larger with regular formation of large-scale flow separation vortices. These observations are in line with typical NACA aerofoil flow phenomena at relatively low Reynolds number [Kim et al.

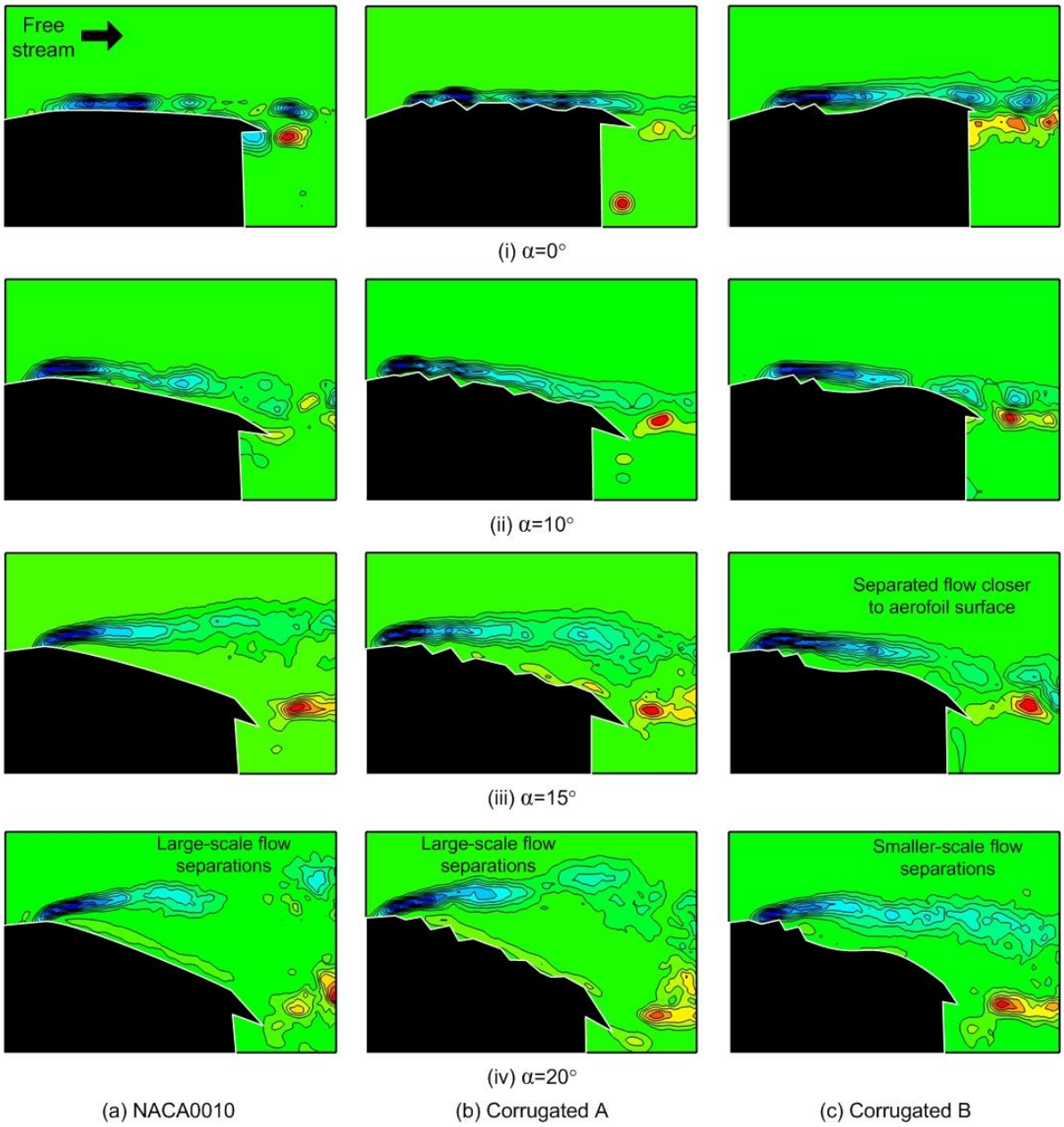

Fig. 4 Reconstructed instantaneous vorticity field maps for (a) NACA0010, (b) Corrugated A and (c) Corrugated B aerofoils at α=0°, 10°, 15° and 20°.

(2011) and Kojima et al. (2013)] and set a benchmark for subsequent comparisons with the corrugated aerofoils.

For Corrugated A aerofoil, Figs. 3(b) and 4(b) show that small-scale flow separations occur at the sharp corrugation peaks along the upper surface at α=0°, and form small recirculating vortices within the valleys. At this angle-of-attack, they are trapped within the valleys and thus do not convect

downstream. Flows further away from the corrugations remain relatively stable and drive the recirculating vortices within the valleys. These observations are consistent with those made by Refs. [9] and [10] earlier. As the angle-of-attack increases to α=10° and 15°, the flow separation behaviour becomes worse than that of the NACA0010 aerofoil at a similar angle-of-attack. The separated flow regions are visually larger and more incoherent. Closer inspection of Figs. 3(b)(ii) and 3(b)(iii) indicates that this is due to strong flow separations occurring immediately along the blunt leading-edge, which are in turn accentuated by the corrugations located downstream. Furthermore, note that the corrugations themselves led to the production of spanwise vorticity, which contributes towards the overall flow separation behaviour.

Recirculating vortices can still be observed to form within the valleys at α=15°, though they now tend to escape the confines of the valleys and merge into the flow separation region. This signifies the increasing ineffectiveness of the corrugations to trap recirculating vortices reliably at higher angles-of-attack under the present test conditions. At α=20°, flow separation region above this aerofoil is comparable to that of the NACA0010 aerofoil and continue to exhibit increased flow incoherence. One likely reason for this observation is that reversed flows at high angles-of-attack will see fluid being directed upstream towards the leading-edge. Unlike the smooth NACA0010 aerofoil, sharp corrugations along the upper surface of Corrugated A aerofoil will lead to multiple minor flow separations and promote flow incoherence as they move upstream. Furthermore, it is also plausible that the comparatively lower Reynolds number used here means that the free stream momentum is not sufficiently strong to deter such behaviour.

Compared to Refs. [9] and [10] where the Reynolds numbers used were much larger, preceding observations show that the use of Corrugated A aerofoil in a significantly lower Reynolds number free-stream does not lead to any significant improvements to the flow separation behaviour, as compared to a NACA0010 aerofoil. In fact, the flow separation region may increase in relative size. Hence, Corrugated A aerofoil is sensitive to the free-stream Reynolds number, where it is more effective at higher Reynolds numbers. This behaviour can be understood if one considers the fact that the size of the flow separation region tends to increase as the Reynolds number is reduced. As

the distance between the corrugations and free stream fluid increases, the ability of the former to induce the latter to move closer to the aerofoil surface will be adversely impacted, as seen in this case. As for Corrugated B aerofoil shown in Figs. 3(c) and 4(c), the flow also separates immediately along the leading-edge at α=0°. The presence of the corrugations again produces recirculating vortices within the valley, as well as the saddle. Due to differences in the size of the valley and saddle, the recirculating vortex formed in the latter will be significantly larger, though its size is constrained by the presence of the trailing-edge hump. As a result, the flow reattaches to the aerofoil upper surface before leaving the aerofoil.

When the angle-of-attack increases to α=10°, this aerofoil continues to limit the growth of the separated flow region through the combined actions of the recirculating vortex at the saddle and trailing-edge hump. In fact, a comparison between all three aerofoils here will show that Corrugated B aerofoil consistently produces the smallest flow separation regions above the aerofoil surface at α=10° and beyond. This is despite that the corrugations in Corrugated B aerofoil produce spanwise vorticity in a relatively similar manner as Corrugated A aerofoil. However, note that the trailing-edge hump has smaller effects in preventing the recirculating vortex from escaping the saddle at higher angles-of-attack. Lastly, it is also interesting to note that flow separation vortices produced along the leading-edge of Corrugated B aerofoil at α=20° tend to be of smaller-scale, compared to both NACA0010 and Corrugated A aerofoils. Generally speaking, the near-wall flow behaviour of the corrugated aerofoils here are comparable to those observed by Refs. [9] to [11], even if their effects on the overall large-scale flow separation behaviour differ.

(ii) Flow separation bubble size

Instantaneous results presented in Figs. 3 and 4 have so far shown that Corrugated B aerofoil exhibits more favourable flow separation control behaviour than Corrugated A aerofoil, and that the latter does not necessarily perform better than NACA0010 aerofoil at the present working conditions. To ascertain that these observations continue to hold true in a more persistent manner, streamlines derived from mean PIV velocity fields are presented in Fig. 5 to inspect the resultant flow separation bubbles. From the figure, recirculating regions are formed above both corrugated aerofoils, particularly for Corrugated B aerofoil. In fact, the recirculating region at the saddle of Corrugated B

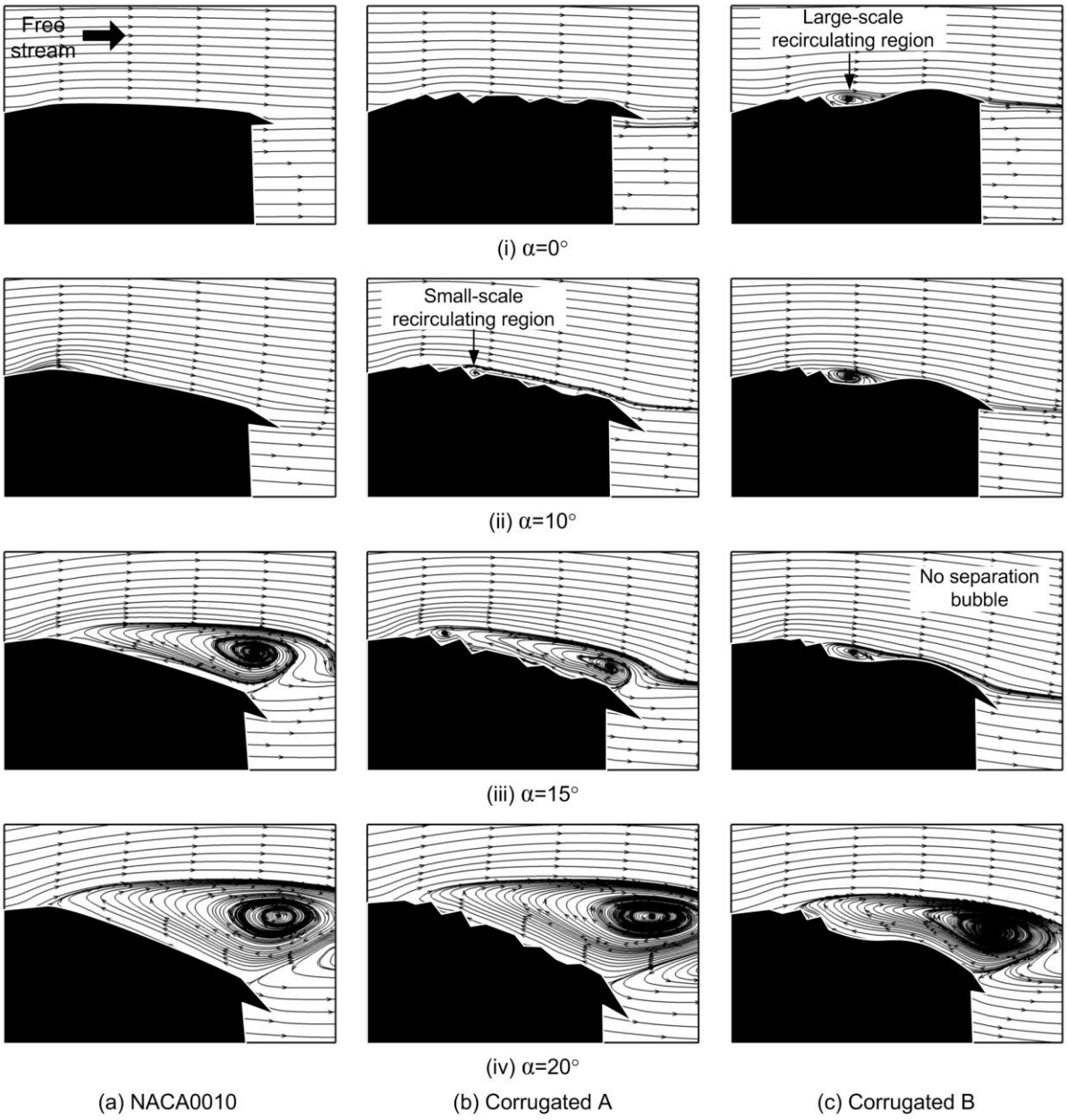

Fig. 5 Mean flow streamlines of (a) NACA0010, (b) Corrugated A and (c) Corrugated B aerofoils at α=0°, 10°, 15° and 20°.

aerofoil can be observed even at α=0°, due to its relatively larger physical size. In contrast, some of the small-scale recirculating regions trapped within the valleys of both corrugated aerofoils are not captured in these streamline results, due to their unsteady nature and limited PIV measurement resolution. Nevertheless, particle-streak visualizations presented earlier have fully ascertained that they are indeed present.

As the angle-of-attack increases to α=10°, at least one of these recirculating regions can be observed within the corrugation valleys in the streamline results of Corrugated A aerofoil. For Corrugated B aerofoil, the large-scale recirculating region remains present and bounded by the trailing-edge hump. In contrast, mean streamlines of NACA0010 aerofoil follow the upper surface closely with no recirculating region formed, as expected. At α=15°, corrugated aerofoils clearly demonstrate their ability in reducing flow separations, with significantly smaller flow separation regions as compared to the NACA0010 aerofoil, especially for Corrugated B aerofoil. Closer inspection reveals that it does not produce a flow separation bubble at all. Other than the recirculating region at the saddle, the flow remains attached to the aerofoil upper surface. This observation supports the earlier notion that the recirculating vortex plays an important role in producing this favourable behaviour. Therefore, it appears that a single but physically larger recirculating region is able to exert more favourable flow influences than multiple, smaller recirculating vortices found in Corrugated A aerofoil. Figure 5(b)(iii) suggests that reversed flows along Corrugated A aerofoil upper surface disrupt the small-scale recirculating regions and render them less effective as the angle-of-attack increases.

At α=20° however, there is no practical difference in flow separation bubble size between NACA0010 and Corrugated A aerofoils, and Corrugated B aerofoil also loses its effectiveness in reducing flow separation bubble size. Result shows that the flow separation region grows dramatically along the Corrugated B aerofoil leading-edge and its recirculating region does not exert significant favourable flow effects, though it still manages to produce the smallest flow separation bubble at this point. Through these preceding comparisons, it is clear that Corrugated B aerofoil is able to limit the size of the flow separation bubble most effectively out of all three test aerofoils up to α=20°, which supports the vortical behaviour presented earlier. Note that Hu and Tamai (2008) had earlier shown that the lift coefficient for their corrugated aerofoil was higher than that of a NACA aerofoil when the corrugated aerofoil produced comparatively smaller flow separation bubbles. Therefore, it is expected that the smaller flow separation bubbles observed in Corrugated B aerofoil here will lead to similar aerodynamic behaviour.

4. Conclusions

Present results show that at Re=14,000, small recirculating vortices within the valleys of Corrugated A aerofoil do not draw free-stream fluid closer to the aerofoil upper surface as well as those observed at significantly higher Reynolds numbers. Therefore, its flow separation bubble sizes are comparable to those for NACA0010 aerofoil. In contrast, Corrugated B aerofoil demonstrates better flow separation control behaviour and as a result, produces significantly smaller flow separation bubbles than Corrugated A and NACA0010 aerofoils. This can be attributed to the formation of a relatively large-scale recirculating region at its saddle location. Results indicate that this physically larger recirculating region works better than multiple small recirculating regions in mitigating flow separation behaviour. Additionally, the trailing-edge hump also enables flow reattachment which reduces flow separation bubble size. While the favourable effects by Corrugated B aerofoil geometry diminish as the angle-of-attack increases, it consistently produces the best flow separation control characteristics among the currently studied aerofoils and test conditions here.

Acknowledgement

The authors wish to acknowledge the support of the study by MINDEF-NTU-JPP/10/09 grant, Undergraduate Research Experience on Campus (URECA) programme of Nanyang Technological University and Advanced Research Programme of NUS High School of Maths and Science.

References

[1]Freymuth, P., "Thrust generation by an airfoil in hover modes," *Experiments in Fluids*, Vol. 9, 1990, pp. 17-24.

[2]Triantafyllou, M.S., Triantafyllou, G.S., and Gopalkrishnan, R., "Wake mechanics for thrust generation in oscillating foils," *Physics of Fluids*, Vol. 3, No. 12, 1991, pp. 2835-2837.

[3]Dickinson, M.H., Lehmann, F-O, and Sane, S.P., "Wing rotation and the aerodynamic basis of insect flight," *Science*, Vol. 284, No. 5422, 1999, pp. 1954-1960.

[4]Ellington, C.P., "Aerodynamics and the origin of insect flight," *Journal of Experimental Biology*, Vol. 202, 1999, pp. 3439-3448.

[5]Lai, J.C.S., and Platzer, M.F., "Jet characteristics of a plunging airfoil," *AIAA Journal* Vol. 37, Issue 12, 1999, pp. 1529-1537.

[6]Wang, Z.J., "Vortex shedding and frequency selection in flapping flight," *Journal of Fluid Mechanics*, Vol. 410, 2000, pp. 323-341.

[7]Sane, S.P., "The aerodynamics of insect flight," *Journal of Experimental Biology*, Vol. 2096, No. 23, 2003, pp. 4191-4208.

[8]Lua, K.B., Lim, T.T., and Yeo, K.S., "Aerodynamic forces and flow fields of a two-dimensional hovering wing," *Experiments in Fluids*, Vol. 45, 2008, pp. 1047-1065.

[9]Hu, H., and Tamai, M., "Bioinspired corrugated airfoil at low Reynolds numbers," *Journal of Aircraft*, Vol.45, No. 6, 2008, pp. 2068-2077.

[10]Murphy, J.T., and Hu, H., "An experimental study of a bio-inspired corrugated airfoil for micro air vehicle applications," *Experiments in Fluids*, Vol. 49, No. 2, 2010, pp. 531-546.

[11]Levy, D-E, and Seifert, A., "Simplified dragonfly airfoil aerodynamics at Reynolds numbers below 8000," *Physics of Fluids*, Vol. 21, 2009, 071901.

[12]Keane, R.D. and Adrian, R.J., "Theory of cross-correlation analysis of PIV images," *Applied Scientific Research*, Vol. 49, No. 3, 1992, pp. 191-215.

[13]Sirovich, L., "Turbulence and the dynamics of coherent structures," *Q Appl Math*, Vol. 45, 1987, pp. 561-590.

[14]Berkooz, G., Holmes, P., and Lumley, J.L., "The proper orthogonal decomposition in the analysis of turbulent flows," *Annual Review in Fluid Mechanics*, Vol. 25, 1993, pp. 539-575.

[15]Chatterjee, A., "An introduction to the proper orthogonal decomposition," *Current Science,* Vol. 78, 2000, pp. 808-817.

[16]Lumley, J.L., "Atmospheric turbulence and radio wave propagation," Edited by Yaglom A. M. and Tatarski V. I., Navko, Moscow, 1967, pp. 160-178.

[17]Aubry, N., Holmes, P., Lumley, J.L., and Stone, E., "The dynamics of coherent structures in the wall region of a turbulent boundary layer," *Journal of Fluid Mechanics,* Vol. 192, 1988, pp. 115-173.

[18]Arndt, R.E., Long, D.F., and Glauser, M.N. "The proper orthogonal decomposition of pressure fluctuations surrounding a turbulent jet," *Journal of Fluid Mechanics*, Vol. 340, 1997, pp. 1-33.

[19]Kim, Y., and Rockwell, D., "Vortex buffeting of aircraft tail: interpretation via proper orthogonal decomposition," *AIAA Journal*, Vol. 43, 2005, pp. 550-559.

[20]Shi, S., New, T.H., and Liu, Y., “Flapping dynamics of a low aspect-ratio energy-harvesting membrane immersed in a square cylinder wake,” *Experimental Thermal and Fluid Science*, In-press, DOI:10.1016/j.expthermflusci.2012.12.007.

[21]Kim, D-H, Chang, J-W, Chung, J., “Low-Reynolds-number effect on aerodynamic characteristics of a NACA 0012 airfoil,” *Journal of Aircraft*, Vol. 48, 2011, pp. 1212-1215.

[22]Kojima, R., Nonomura, T., Oyama, A., and Fujii, K., “Large-eddy simulation of low-Reynolds-number flow over thick and thin NACA airfoils,” *Journal of Aircraft*, Vol. 50, pp. 187-196.